

7-29-2019

## Development of helical, fish-inspired cross-step filter for collecting harmful algae

Adam Schroeder

Lauren Marshall

Brian Trease

Anna Becker

S. Laurie Sanderson

*William and Mary*, [slsand@wm.edu](mailto:slsand@wm.edu)

Follow this and additional works at: <https://scholarworks.wm.edu/aspubs>



Part of the [Animal Experimentation and Research Commons](#), and the [Marine Biology Commons](#)

---

### Recommended Citation

Schroeder, Adam; Marshall, Lauren; Trease, Brian; Becker, Anna; and Sanderson, S. Laurie, Development of helical, fish-inspired cross-step filter for collecting harmful algae (2019). *Bioinspiration & Biomimetics*, 14(5).

<https://scholarworks.wm.edu/aspubs/1055>

This Article is brought to you for free and open access by the Arts and Sciences at W&M ScholarWorks. It has been accepted for inclusion in Arts & Sciences Articles by an authorized administrator of W&M ScholarWorks. For more information, please contact [scholarworks@wm.edu](mailto:scholarworks@wm.edu).

ACCEPTED MANUSCRIPT

## Development of helical, fish-inspired cross-step filter for collecting harmful algae

To cite this article before publication: Adam Schroeder *et al* 2019 *Bioinspir. Biomim.* in press <https://doi.org/10.1088/1748-3190/ab2d13>

### Manuscript version: Accepted Manuscript

Accepted Manuscript is “the version of the article accepted for publication including all changes made as a result of the peer review process, and which may also include the addition to the article by IOP Publishing of a header, an article ID, a cover sheet and/or an ‘Accepted Manuscript’ watermark, but excluding any other editing, typesetting or other changes made by IOP Publishing and/or its licensors”

This Accepted Manuscript is © 2019 IOP Publishing Ltd.

During the embargo period (the 12 month period from the publication of the Version of Record of this article), the Accepted Manuscript is fully protected by copyright and cannot be reused or reposted elsewhere. As the Version of Record of this article is going to be / has been published on a subscription basis, this Accepted Manuscript is available for reuse under a CC BY-NC-ND 3.0 licence after the 12 month embargo period.

After the embargo period, everyone is permitted to use copy and redistribute this article for non-commercial purposes only, provided that they adhere to all the terms of the licence <https://creativecommons.org/licenses/by-nc-nd/3.0>

Although reasonable endeavours have been taken to obtain all necessary permissions from third parties to include their copyrighted content within this article, their full citation and copyright line may not be present in this Accepted Manuscript version. Before using any content from this article, please refer to the Version of Record on IOPscience once published for full citation and copyright details, as permissions will likely be required. All third party content is fully copyright protected, unless specifically stated otherwise in the figure caption in the Version of Record.

View the [article online](#) for updates and enhancements.

# Development of Helical, Fish-Inspired Cross-step Filter for Collecting Harmful Algae

Adam Schroeder<sup>1</sup>, Lauren Marshall<sup>1</sup>, Brian Trease<sup>1</sup>, Anna Becker<sup>2</sup>, and S. Laurie Sanderson<sup>3</sup>

<sup>1</sup> Department of Mechanical, Industrial, and Manufacturing Engineering, University of Toledo, Toledo OH, USA

<sup>2</sup> Department of Mechanical and Aerospace Engineering, University of Alabama in Huntsville, Huntsville AL, USA

<sup>3</sup> Department of Biology, College of William and Mary, Williamsburg VA, USA

E-mail: adam.schroeder@utoledo.edu

Received xxxxxx

Accepted for publication xxxxxx

Published xxxxxx

## Abstract

A new filter was developed to collect harmful algae colonies by adapting the cross-step filtration structures and mechanisms discovered recently in filter-feeding fish. Extending beyond previously published models that closely emulated the basic morphology of the fish, the new cross-step filter's major innovations are helical slots, radial symmetry, and rotation as an active anti-clogging mechanism. These innovations enable the transport of concentrated particles to the downstream end of the filter. This advance was made possible by recognizing that biologically imposed constraints such as bilateral symmetry do not apply to human-made filters. The use of helical slots was developed in a series of iterative tests that used water-tracing dye and algae-sized microspheres. The major products of the iterative tests were refinements in the helical design and an understanding of how varying the major structural parameters qualitatively influenced fluid flow and filter performance. Following the iterative tests, the clogging behavior of select filters was quantified at high particle concentrations. Vortices in the helical filter were effective at reducing clogging in the center of the slots. By considering the design space that is free of the biological constraints on the system and exploring the effects of variations in major structural parameters, our work has identified promising new directions for cross-step filtration and provided key insights into the biological system.

Keywords: vortical cross-step filtration, harmful algal blooms (HABs), helical filter, filter-feeding fish, crossflow filtration, backward-facing step, bioinspired

## 1. Introduction

Harmful algal blooms (HABs) are massive populations of microalgae which can contaminate drinking water, create anoxic conditions, and/or contain an intracellular toxin (Kudela et al 2015; Paerl 2014). These species of algae take different forms, but one of the most problematic freshwater species, *Microcystis aeruginosa*, is a cyanobacterium (blue-green alga) that forms colonies ranging in size from 20-

700µm (Zhu et al 2014). These blooms occur globally and can be a byproduct of excessive nutrients running off into rivers and lakes. Stemming the flow of these nutrients is a long-term, difficult task (International Joint Commission 2014). A more immediate solution would be to physically remove harmful algae from water.

Filter-feeding fish can collect zooplankton and phytoplankton such as microalgae efficiently from enormous

1  
2  
3 volumes of water. Ram filter-feeding fish such as anchovies,  
4 mackerel and menhaden swim with their mouths open,  
5 allowing them to continuously separate food particles from  
6 water (Sanderson and Wassersug 1993).

7 An active area of research involves exploring the  
8 mechanisms used by ram filter-feeding fish to collect small  
9 particles without clogging. Fouling of the filter with particles  
10 or solutes is a major limitation of many industrial filtration  
11 processes (Imbrogno and Belfort 2016; Jaffrin 2012).  
12 Previous research by one of the authors introduced a new  
13 filtering mechanism called vortical cross-step filtration based  
14 on physical models of ram filter-feeding fish (Brooks et al  
15 2018; Sanderson et al 2016). The basic cross-step filter  
16 design published by Sanderson et al (2016) has been  
17 proposed for the adsorption of biological macromolecules  
18 (Zhou et al 2018). Here, by modifying the basic design  
19 substantially, we apply the cross-step filtration mechanism to  
20 the particular application of collecting algae from harmful  
21 algal blooms.

22 Our new work takes advantage of the freedom from  
23 biologically imposed constraints. For example, fish typically  
24 exhibit bilateral symmetry, which limits how these filter-  
25 feeding mechanisms can be employed. Removing such  
26 biologically imposed constraints, while necessarily imposing  
27 new engineering constraints, expands the design space. A  
28 major novel contribution of this work, which will be  
29 explained in more detail, is the addition of a helical-shaped  
30 slot. This helical slot still uses the same cross-step filtering  
31 mechanism as the fish but is not bilaterally symmetric.

32 Throughout this work, several examples are given of how  
33 the desired bioinspired mechanism can be extended, or how  
34 simpler engineering solutions can be substituted in place of  
35 more complex biological behaviors and structures. For  
36 example, ram filter feeders exhibit a yaw movement (Carey  
37 and Goldbogen 2017; Haines and Sanderson 2017) and can  
38 dynamically reshape movable bony structures or flexible soft  
39 tissue (Sanderson et al 1994; Sanderson and Wassersug  
40 1993), which may reduce clogging of the filter and also  
41 transport concentrated particles downstream inside the filter.  
42 An engineering approach has the freedom to substitute less  
43 complex behaviors and structures, while achieving similar  
44 outcomes.

45 Our research initially employed an iterative design  
46 approach. Many iterative changes in the physical models  
47 were used to isolate the impacts that specific geometrical  
48 parameters have on fluid and particle movements. Knowledge  
49 of the impacts of varying these individual parameters was  
50 leveraged to develop a filter that can take advantage of the  
51 previously described anti-clogging properties of cross-step  
52 filtration (Sanderson et al 2016), while building in new  
53 anti-clogging features. Following this iterative design phase,  
54 a more focused round of clogging tests was performed for  
55 select filters.

The remainder of this work is organized as follows. Section 2 gives background information on ram filter feeders, as well as key previous work from the authors. Section 3 describes the methodologies used, as well as details of the iterative design process and clogging tests. Section 4 discusses the results of these iterative and clogging tests, reflects on the insights this research gives into how the original biological system functions, and introduces ongoing and future work to apply the cross-step filters for the control of harmful algal blooms. Finally, Section 5 concludes and offers thoughts on the most promising areas for future work.

## 2. Background

The basis for this work is the previous introduction of the vortical cross-step filtration mechanism (Brooks et al 2018; Sanderson et al 2016). This filtering mechanism uses a series of solid ribs that form the wall of a porous channel or pipe, with consecutive ribs spaced a relatively short distance apart ( $d$ -type roughness, characterized by an aspect ratio of slot width to rib height  $\sim 3$ -4, Liu and Chung 2012; Stel et al 2012). The downstream wall of each solid rib forms a backward-facing step, as shown in Figure 1. A permeable mesh is mounted across the external margins of consecutive steps, forming deep slots inside the filter in which a recirculation zone, i.e., vortical flow, is generated and sustained as water exits from the filter via the slots. This recirculation zone is caused by the flow separation occurring downstream of each backward-facing step (Liu and Chung 2012). The resulting shear layer and vortex continuously scour the mesh along the center of the slot, which delays the onset of clogging (Brooks et al 2018). In fish, the backward-facing steps could be formed by the branchial arches and/or the gill rakers (Sanderson et al 2016).

The development of cross-step filtration was dependent on earlier reports of crossflow that travels tangentially across the filter elements towards the esophagus located at the posterior of the oral cavity (Callan and Sanderson 2003; Cheer et al 2012; Cohen et al 2018; Motta et al 2010; Paig-Tran et al 2013; Sanderson et al 2001). Prior to the discovery of crossflow filtration in fish (Brainerd 2001; Sanderson et al 2001), the assumption was that filter-feeding fish used primarily dead-end sieving, in which the flow passes perpendicularly between the filter elements. However, dead-end sieving could not explain the lack of clogging on the filtration surfaces of fish, nor account for the transport of retained particles towards the esophagus for swallowing (Sanderson and Wassersug 1990; Sanderson and Wassersug 1993).

Even in industrial crossflow filtration, however, fouling of the filter is a major problem (Jaffrin 2012). Cross-step filtration provides a mechanism for the concentration, suspension, and transport of particles with a reduction in clogging (Sanderson et al 2016). In cross-step filtration,

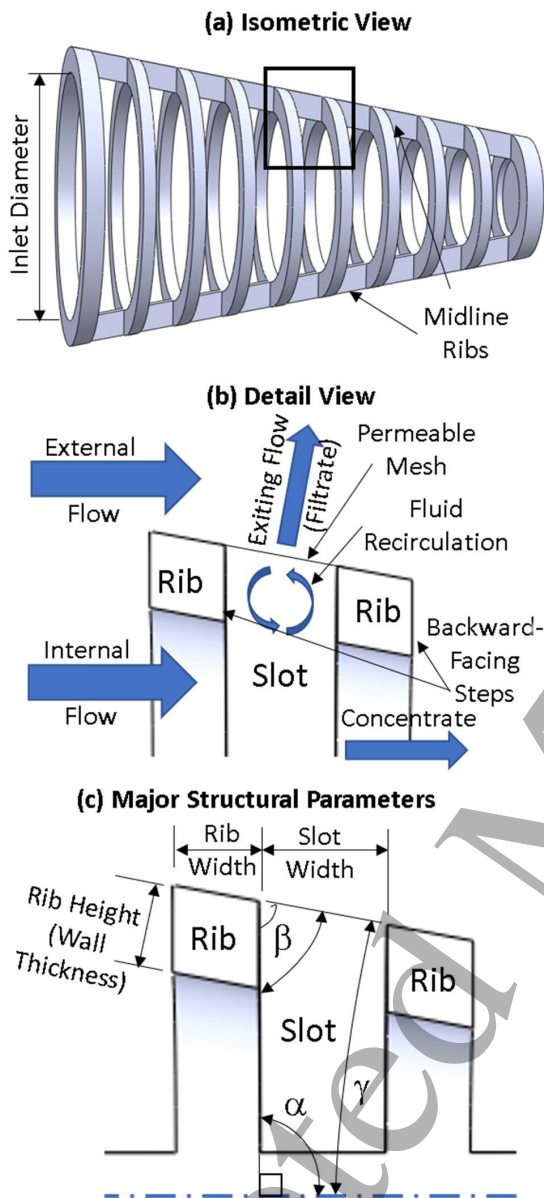


Figure 1: (a) Isometric view of a cross-step filter, with (b) a longitudinal-section view from the box in part a, showing the flow, the ribs that form backward-facing steps, and the location of the permeable mesh, and (c) major structural parameters of cross-step filters, including slot angle ( $\alpha$ ), rib angle ( $\beta$ ), and conical angle ( $\gamma$ ). In the basic cross-step filter, the three angles are related as  $\beta = 180^\circ - \alpha - \gamma$

mainstream flow enters the inlet of the model, then travels tangentially across the series of *d*-type ribs, and exits through the slots between the ribs. The ribs in a cross-step filter form backward-facing steps that generate vortices to shear

particles from the mesh surface and suspend and transport particles inside the slots. In paddlefish and basking sharks, the backward-facing steps are formed by cartilaginous branchial arches inside the mouth. Instead of a mesh, these fish species use porous gill rakers that are attached to the external surfaces of their branchial arches.

The distinction between *d*-type and *k*-type roughness is used frequently in describing the fluid mechanics of ribbed surfaces that are solid rather than porous. On solid ribbed surfaces such as the cooling ducts of gas turbines, the width of the groove or slot between the *k*-type ribs is large compared to the rib height (aspect ratio of slot width to rib height  $\gg 4$ , Liu and Chung 2012; Stel et al 2012). Therefore, the shear layer that separates from the downstream edge of each *k*-type rib reattaches to the bottom of the solid groove between two consecutive ribs (Leonardi et al 2003; Narasimhamurthy and Andersson 2015). In contrast, in *d*-type roughness, the width of the slot between ribs is small compared to the rib height (aspect ratio of slot width to rib height  $\sim 3$ -4, Liu and Chung 2012; Stel et al 2012; Figure 1). Therefore, the shear layer and associated recirculation zone extend across the width of the slot between consecutive *d*-type ribs. Heat exchangers use *k*-type ribs to enhance heat transfer by increasing local turbulence, but the use of *k*-type ribs in cross-step filtration would cause the porous surface of the filter to clog where the separated shear layer reattaches to the bottom of the slot, because the anti-clogging effects of the recirculation zone would not extend to that location.

Previous physical models for cross-step filtration (Brooks et al 2018; Haines and Sanderson 2017; Marshall et al 2018) mimicked the morphology of paddlefish and basking sharks. These previous filters had five slots, where the groove aspect ratio (slot width divided by rib height) was chosen to imitate the *d*-type ribs of these fish. Marshall et al (2018) specifically explored the impact of packaging these five slots in different forms including conical, square, elliptical (imitating a manta ray), and conical with V-shaped lateral cutouts at the inlet (to more closely imitate the shape of a fish's gape). Later analysis of these geometries revealed that the fluid exit ratio (defined by Brooks et al as the ratio of exit area through the slots to inlet area of the model) was too low for each of these cross-step models. The previous filters of Marshall et al did capture particles, but later testing revealed that significant vortices were not present in the slots. In our current work, improved (higher) fluid exit ratios were integral to the design of filters that generate vortical flow for cross-step filtration.

A generic version of the slot geometry of the filters tested in new and previous work is shown in Figure 1c. This figure illustrates some of the major structural parameters of interest in cross-step filters, including slot angle ( $\alpha$ ), rib angle ( $\beta$ ), and conical angle ( $\gamma$ ). The slot angle denotes the angle at which the slot intersects the axis of the model. The rib angle

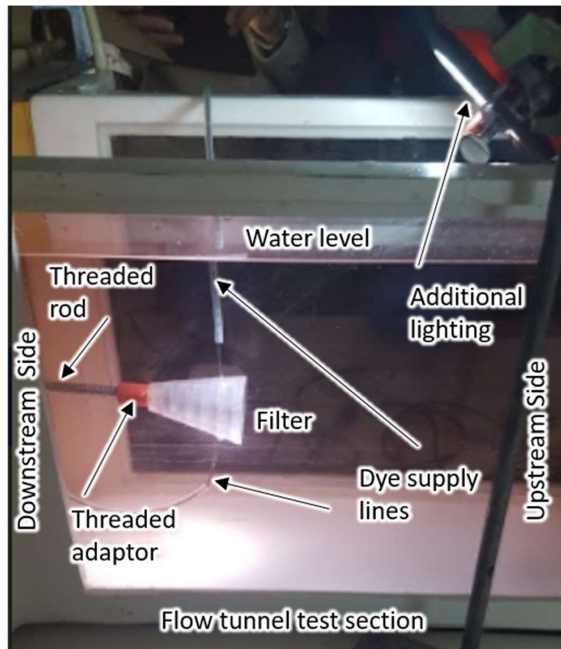


Figure 2: Flow tunnel test section and filter mounting fixture

provides information about the orientation of the wall that forms the margin of the slot. The conical angle denotes the angle of the cone with respect to the centerline of the model. Since fish can use muscles to adjust these three angles during feeding, our models have explored some of the effects of variation in these angles (Table 1, Figure 15).

### 3. Methodology and Iterative Development

Experiments were conducted using a flow tunnel with a 19 cm wide x 28cm deep x 46 cm long test section. All tests were run with the flow tunnel set to 14 cm/s. Filters were mounted in the center of the flow tunnel using a rigid threaded rod, as shown in Figure 2. Small 3D-printed adaptors were adhered to the back of a filter, and then threaded onto the rod. Both water-tracing dye and microspheres were used to visualize flow and evaluate particle accumulation on the filter. Dye was injected using a syringe and small tube that was inserted into a hole drilled in the filter frame. The microspheres (Cospheric fluorescent green polyethylene microspheres, 106-125 $\mu\text{m}$  diameter, 1.00g/cc) were chosen to be comparable to *Microcystis* colonies. Chaffin et al (2011) reported that 93% of the *Microcystis* cells collected from Lake Erie water samples at 1 m depth and filtered through a series of mesh sizes (112  $\mu\text{m}$ , 53  $\mu\text{m}$ , and 30  $\mu\text{m}$ ) were in the form of colonies > 112  $\mu\text{m}$  in diameter. *Microcystis* cells contain a gas vacuole that can counteract the density of the cell contents and cause colonies to form positively buoyant flocs (Nakamura et al 1993). Rowe et al (2016) reported that *Microcystis* colonies in Lake

Erie can concentrate on the surface, as well as be distributed vertically during mixing events. They found that the median *Microcystis* colony diameter in Lake Erie was 117  $\mu\text{m}$ .

The Cospheric microspheres fluoresce green when excited with UV-light, which enhanced the visibility of deposited particles in the flow tunnel experiments. Additional lighting was provided by either an LED flashlight, for the dye experiments, or a tube blacklight, for visualizing the particles. Images were captured using a Huawei KIW-L24 16MP camera and video was acquired with the same camera at 30 fps with a resolution of 1080p.

The filters themselves were fabricated using clear resin in a Stereolithographic (SLA) 3D Printer (Form Labs 2). After the recommended post-processing, sections of nylon mesh used for plankton nets (100-micron pore size, 44% open area, Sefar Nitex) were hand-fitted and adhered (Gorilla Glue Clear Epoxy) to the 3D-printed frame. The mesh typically had to be epoxied in at least two steps, where some filter geometries required the mesh to form a small overlap.

In cross-step filtration, a recirculation region forms on the downstream side of each rib (Figure 1b). As discussed by Brooks et al (2018), structural features of cross-step filters can trap a stable vortex within the slot downstream from each

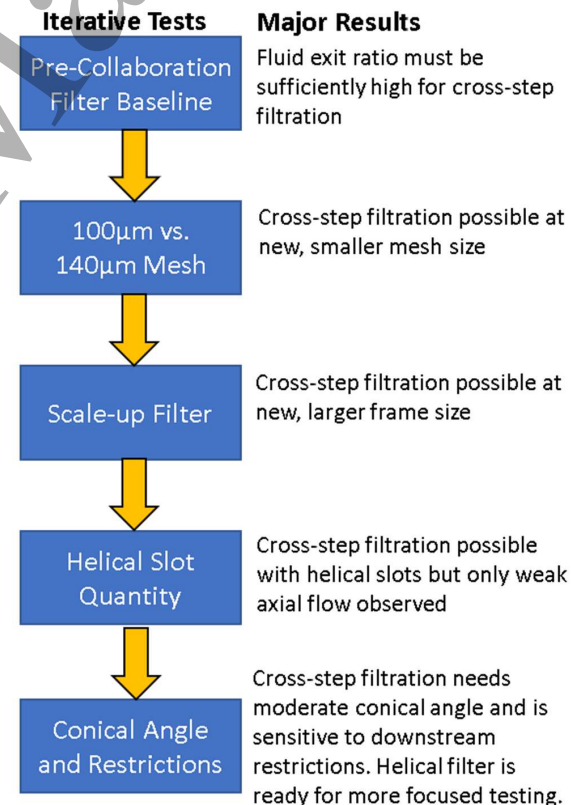


Figure 3: Flowchart of iterative tests (blue boxes) with major results listed to the right.

rib, preventing the bursting of the vortex through the mesh. For these vortices to reduce clogging and transport particles inside the filter, (1) the vortex diameter must extend into the slot to scour the filtration surface between consecutive ribs (Figure 1b), (2) the vortex must travel along the slot between ribs rather than simply remaining stationary, and (3) the vortex must be stable and sustained within the slot rather than dissipating rapidly and exiting through the mesh. Adapting the methodology of Brooks et al (2018), the three vortex parameters above were assessed qualitatively from the dye flow visualization.

The following sections and subsections will describe the sequence of iterative tests and clogging tests, along with test-specific methodologies. The iterative tests used dye and low concentrations of microspheres in the flow tunnel whereas the clogging tests used high concentrations of microspheres. A comprehensive list of the filters tested, and their major structural dimensions, is given in Table 1 for reference.

**3.1 Iterative Tests:** A flowchart of the sequence of iterative tests in Figure 3 shows the logical experimental progression. The major iterative steps were (i) performing a baseline of the pre-collaboration filters, (ii) comparing different meshes, (iii) scaling the filter's frame, (iv) transitioning from a conventional slot layout to a helical slot, and (v) varying the conical angle and removing downstream restrictions. Figure 3 also summarizes the major results from each step in the iterative process, detailed below.

**3.1.1 Baseline: Pre-Collaboration Filters:** As a baseline, previously tested filter geometries from Marshall et al (2018) and Sanderson et al (2016) were run, as shown in Figure 4. The Marshall filter used 100 $\mu$ m mesh to capture the 106-125 $\mu$ m microspheres, whereas the Sanderson filter used 140 $\mu$ m mesh to capture 210-300 $\mu$ m particles. Vortices in the

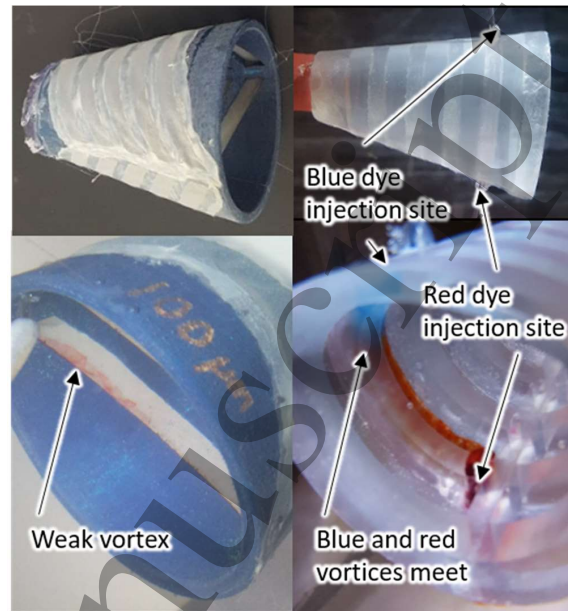


Figure 4: Baseline tests of pre-collaboration filters (left) Marshall et al (2018) and (right) Sanderson et al (2016).

slots were observed in both filters, but the vortices were larger in diameter and much more stable in the Sanderson filter.

There was a vast disparity between the fluid exit ratios for these two filters (Marshall 0.66, Sanderson 1.48, Table 1). The 100 $\mu$ m mesh only had 44% open area, less than the 55% open area for the 140 $\mu$ m mesh, which contributed to the disparity. The higher fluid exit ratio in the Sanderson filter was correlated with the formation of larger sustained vortices, as predicted by Brooks et al (2018).

TABLE 1: Filters Tested

Figure #	Fluid Exit Ratio	Helical	Helix Pitch [mm]	Inlet Diameter [mm]	Conical Angle [deg]	Cone Length [mm]	Rib Height [mm]	Slot Width [mm]	Mesh Pore Size [ $\mu$ m]
4 (left)	0.66	No	N/A <sup>1</sup>	67	12.07	87.7	3.9	6.9	100
4 (right)	1.48	No	N/A	40 <sup>2</sup>	9.4-16.8	61	3.7-6.7	6.1-6.9	140
5 (not shown)	1.16	No	N/A	40	10.5	96	4	6	100
5 (shown)	1.45	No	N/A	40	10.5	96	4	6	140
6, 10 (top), 11 (left), 12 (top), 16	1.49	No	N/A	80	10.5	152	8	12	100
7 (top)	1.08	1 Helix	10	40	10.5	96	4	6	100
7 (mid-top)	1.48	4 Helices	40	40	10.5	96	4	6	100
7 (middle), 9	1.21	6 Helices	60	40	10.5	96	4	6	100
7 (mid-bottom)	1.20	8 Helices	80	40	10.5	96	4	6	100
7 (bottom)	1.64	8 Helices	80	40	5.5	96	4	6	100
9 (top)	1.44	8 Helices	120	80	10.5	152	8	12	100
9 (middle), 14	1.26	8 Helices	120	80	13	167.5	8	12	100
9-10 (bottom), 11 (right), 12 (bottom), 13	1.57 <sup>3</sup>	8 Helices	120	80	10.5	167.5	8	12	100
10-12 (middle)	2.00	No	N/A	80	10.5	152	8	N/A	100

<sup>1</sup> N/A = not applicable

<sup>2</sup> Inlet not circular. Hydraulic diameter is 40mm.

<sup>3</sup> Open slot outlets at rear of filter included in ratio calculation.

3.1.2 *Compare 100 $\mu$ m and 140 $\mu$ m Mesh:* Next, the Marshall filter was modified to improve its fluid exit ratio by extending the filter frame and adding additional slots (nine instead of five). In this second test, a version with a 100 $\mu$ m mesh and a 140 $\mu$ m mesh were run, and strong, robust vortices were observed in the slots of both, with one filter shown in Figure 5 (top) and Supplementary Video 1. These filters had a fluid exit ratio of 1.16 and 1.45, respectively. For all subsequent tests, only 100 $\mu$ m mesh was used because the 140 $\mu$ m mesh is not small enough to capture the algae-sized microspheres.

Not only were the vortices observed using dye, but particles accumulated on the upstream and downstream sides of the slots, while keeping the middle of the slot free from particles, shown in Figure 5 (bottom). This is the expected particle deposition pattern when vortices are present (Sanderson *et al* 2016), but this deposition pattern had not been observed previously with these particles (106-125 $\mu$ m diameter; Marshall *et al* 2018), which are smaller than the

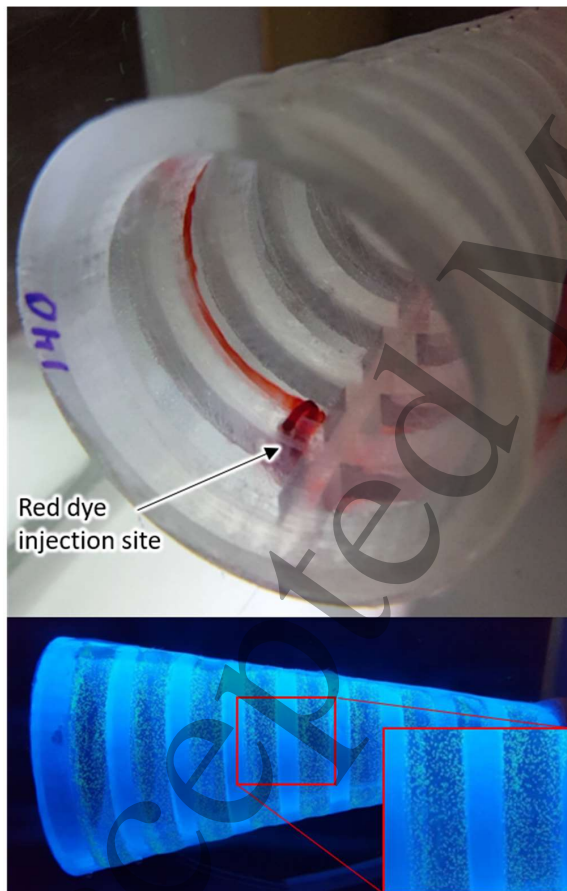


Figure 5: (top) Vortices were observed for both the 100 and 140  $\mu$ m mesh filters with higher fluid exit ratios (140  $\mu$ m mesh shown), and (bottom) the mesh in the center of the slots accumulated less particles, due to the vortices.

particles used in Sanderson's earlier testing (210-300 $\mu$ m diameter).

These filters served as a basis for future tests, with a 10.5° conical angle, 6mm-wide slots, 4mm-thick walls, 4mm-wide ribs, 96mm-length cone, and a 40mm-diameter inlet. This slot width and wall thickness combination gives a *d*-type aspect ratio of 1.5 for the slot width to rib height, which was maintained for all tests.

3.1.3 *Scale-up 40mm to 80mm Inlet:* The next round of tests aimed to determine whether cross-step filtration was possible when doubling the filter size. It was not necessarily important that the filter worked at this exact size, but rather that the filter could be scaled to any desired size. A new filter was created with an 80mm-diameter inlet, 12mm-wide slots, 8mm-thick walls, and a resulting 1.49 fluid exit ratio. This filter was 152mm-long, which is not twice as long as the filter on which it was based (section 3.1.2) because the rib width was not modified.

Large, steady vortices were also observed at this larger scale, as shown in Figure 6. Using the height of the backward-facing step (i.e. rib height) as the characteristic dimension and the free speed of water in the flow tunnel, the Reynolds number (*Re*) for the 40mm and 80mm-inlet filters

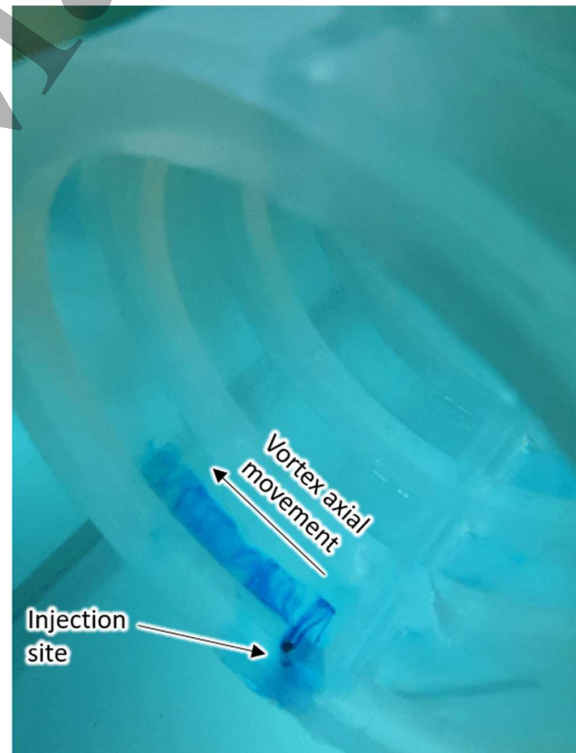


Figure 6: Large, steady vortices were still generated when the inlet diameter was increased from 40mm to 80mm (shown).



was 558 and 1116, respectively. Using the diameter of the filter inlet as the characteristic dimension, the  $Re$  was 3028 and 6056, respectively.

To this point, the viability of collecting microspheres had been established and particle deposition patterns had indicated that the vortices were keeping the mesh in the center of the slots clear, which should delay clogging. However, without a means to transport particles away from the slots, the filter would eventually clog.

**3.1.4 1x, 4x, 6x, or 8x Helical Slots:** To enhance the axial transport of concentrated particles within the slots, a new type of filter was designed that replaced the individual, vertical slots with one or several helical slots. As in Figure 6, the vortices in previous, non-helical filters had been observed to travel axially, inside their slots (Brooks et al 2018), and to transport suspended particles in some cases (Sanderson et al 2016). However, in fish as well as in the non-helical filters, the slots do not extend continuously from the inlet of the filter to the downstream end. The intent behind the new helical slots was that travel of the vortex along its axis within the slots would enable transport of particles from the upstream inlet of the filter to the downstream end.

To achieve continuous particle transport toward the downstream end of the filter, the bilateral symmetry of the earlier non-helical models was replaced with the radial symmetry of the helical slots. All of the filter geometries from Marshall et al (2018) and Sanderson et al (2016) have two solid midline regions, or longitudinal ribs, extending from the inlet of the model to the downstream end of the model (see Figure 1a). These solid midlines mimic solid regions on the dorsal roof and ventral floor of all fish mouths, which divide the fish mouth into a right side and a left side. Freedom from this biologically imposed design constraint enabled the removal of these solid midline regions from our subsequent models. Filters with a 40mm-inlet and a single helix, and with four, six, or eight helices, were tested, shown sequentially in Figure 7. All helical filters had clockwise helices when viewed from the filter inlet.

Unlike previous filters, the helical filters had an effective slot angle ( $\alpha$ , Figure 1c) that was not  $90^\circ$ . The magnitude of the slot angle varied between models depending on the helix pitch, which was adjusted to accommodate the number of helical slots. The helix for the single helix version had a 10mm-pitch, and adding additional helices proportionally increased the pitch, e.g. the eight-helix variant had an 80mm-pitch. The slot angle is a function of the helix pitch,  $P$ , which was constant within a model, and the filter outer diameter,  $D$ , which varied within a model depending on the outer diameter of the cone at the slot angle vertex. That is, the slot angle decreased from the upstream end of the model to the downstream end, as shown in Figure 8. The effective slot angle can be calculated at any point along the cone using Equation 1.



Figure 7: Filters were tested with 1x, 4x, 6x or 8x helical slots.

$$\alpha = \tan^{-1} \frac{\pi D}{P} \quad (1)$$

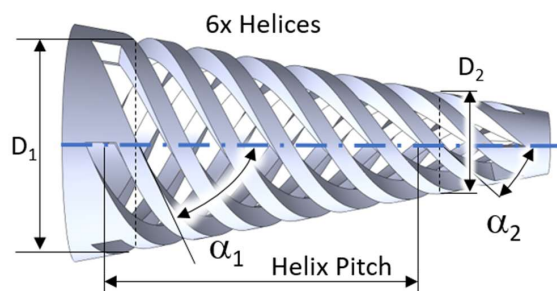


Figure 8: The helix pitch was constant within a model, but the slot angle ( $\alpha$ ) varied within each model depending on the outer diameter of the cone ( $D$ ).

Vortices were observed in the slots of each of the helical filters depicted in Figure 7, but the vortex did not travel axially along the entire length of the helical slots. Note, however, that the recirculation region is generated downstream of each backward-facing step throughout cross-step filters, even when the vortex does not travel axially. It was hypothesized that the single helix version did not have an aggressive enough slot angle, i.e. alpha was too big, to induce the vortex to travel axially along the length of the helical slot. For the multi-helix filters, the vortices were observed to travel axially, but then eventually terminate near the middle or downstream end of the filter. It was hypothesized that these filters had an appropriate slot angle on the upstream end of the filter, but a slot angle that was too aggressive, i.e. alpha too small, on the downstream end of the filter.

An attempt was made to increase the magnitude of the slot angle on the downstream end of an eight-helix filter by decreasing the conical angle from  $10.5^\circ$  to  $5.5^\circ$ , shown in Figure 7 (bottom). Vortices were observed in this filter, but they were small in diameter relative to the width of the slot and did not have a strong axial component. Particle deposition patterns also indicated only weak vortices, predominately on the upstream end of the filter.

**3.1.5 Conical Angle and Downstream Restrictions:** The last iterative test set focused on addressing issues from the initial round of helical filter testing. All filters had an 80-mm diameter inlet and had eight helices. As for the previous 80mm-inlet non-helical filter, slot widths were doubled to be 12mm-wide and the filter walls were 8mm-thick. A helix pitch of 120mm was used at this new size, to achieve a similar slot angle to the eight-helix, 40mm-inlet filters, which had a pitch of 80mm.

Surprisingly, the double-scale version of the eight-helix filter had strong vortical movement from the downstream end of the filter to the upstream end, shown in Figure 9 (top). This is the opposite direction of what was intended for particle transport. It was hypothesized that doubling the scale

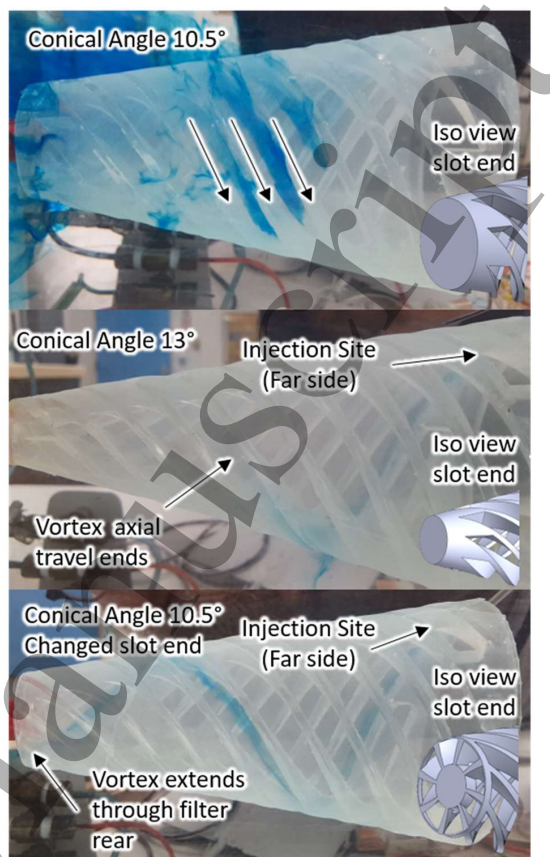


Figure 9: The conical angle and downstream geometry of the helical slots were varied, which influenced the direction and extent of axial flow within the slots.

also increased the flow restriction caused by the dead-end downstream end of the filter.

Another filter was constructed, shown in Figure 9 (middle), with a  $13^\circ$  conical angle instead of  $10.5^\circ$ , which decreased the diameter of the dead-end downstream end of the filter. This conical angle adjustment changed the axial movement of the vortices back to the intended direction, upstream-to-downstream. However, as with the smaller helical filters from the previous round of testing, these vortices still did not travel the entire length of the helical slot.

Different options were then explored for how the helical slots terminated at the downstream end of the filter. To this point, the helical slots had always ended immediately before the very back of the filter, as visible in Figure 8. Another filter was created instead, where the slots were extended to cut through the back wall of the filter, shown in Figure 9 (bottom). This filter, which returned to the original  $10.5^\circ$  conical angle, was finally able to generate a vortex which traveled inside the entire length of the helical slot (Supplementary Video 2). This movement of the vortex from

the entrance of the model to the open downstream end of the filter is significant because such vortical flow could be manipulated to suspend and transport particles along the entire length of the model. Therefore, the collection of concentrated particles from the rear of the filter might be feasible, potentially enabling continuous filtration without clogging.

**3.2 Clogging Tests:** The iterative testing had developed a helical filter that could generate a continuous vortex moving axially from the upstream inlet of the filter to the downstream end (Figure 9 bottom). This next series of tests focused on evaluating the clogging behavior of this promising design and comparing it to a non-helical cross-step filter and to a filter that does not use cross-step filtration. The filters were first tested as they *passively* collected particles, i.e. were held in a fixed position in the flow tunnel. After this, *active* collection strategies were explored, i.e. strategies that moved the filter to redistribute particles that had already been collected.

**3.2.1 Passive Collection Tests:** During passive collection tests, filters were held in a fixed position, which is simpler than the case of ram filter-feeding fish. Unlike the live fish, the passive filters were not performing a yaw movement (Carey and Goldbogen 2017; Haines and Sanderson 2017) nor was the structure being dynamically reshaped (Sanderson et al 2016, 1994). Two filters from the previous tests were used, both with an 80mm-diameter inlet and a 10.5° conical angle: (1) a filter with nine non-helical slots (Figure 6), and (2) a filter with eight helical slots (Figure 9 bottom). A third, ‘conventional filter’ was also tested, which did not have any slot features. This filter was designed to use only normal crossflow filtration and did not have any bioinspired features. It had the same conical angle and inlet diameter as the two bioinspired cross-step filters. This conventional filter is comparable to plankton nets that are regularly used to collect algae samples in the field (Bridgeman et al 2013). The nets are also comparable to those used by some of the authors to collect algae using a swarm of robot boats (Schroeder et al 2018).

For these tests, the flow tunnel was seeded with 5g of the Cospheric microspheres, and each filter was placed in the flow tunnel for 10 minutes. Images of the filters were taken at 1, 2, 3, 4, 5, 7.5 and 10 minutes. A subset of these images is shown in Figure 10. In the cross-step filters, the vortices did scour the center of the slots, keeping these locations unclogged for a period of time (Figure 10, top and bottom). There is also an area of mesh immediately downstream of the inlet on the conventional filter that had delayed clogging (Figure 10 middle - 2 and 3 minutes). This is because the inlet of this filter itself forms a backward-facing step. A recirculation zone forms behind the inlet, which keeps the mesh in this area clear of particles.

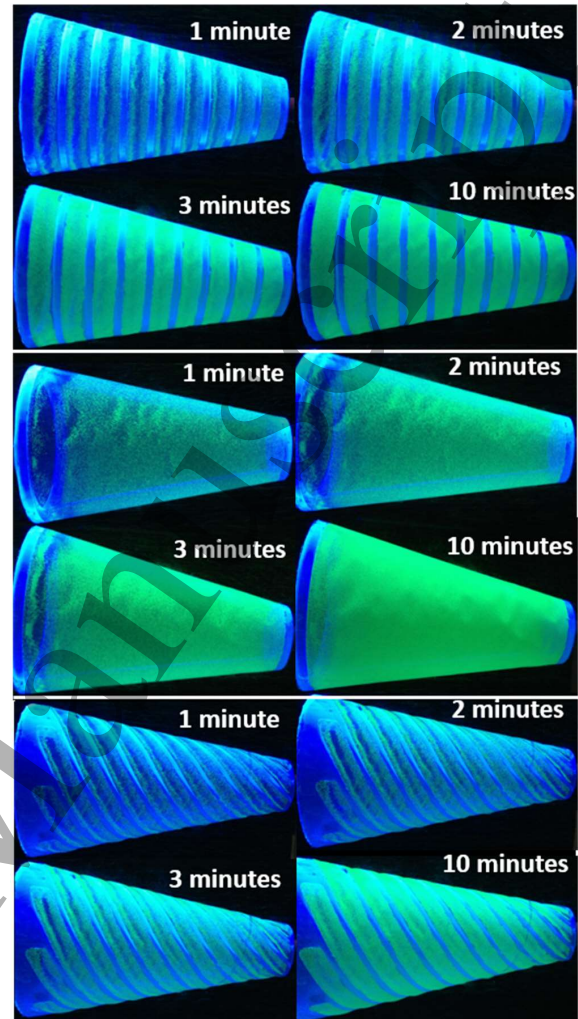


Figure 10: Progressive clogging at high particle concentrations in passive collection tests after 1, 2, 3, and 10 minutes for the: (top) non-helical cross-step filter, (middle) conventional filter without cross-step filtration, and (bottom) helical cross-step filter.

The images of the filters were processed to quantify the extent of clogging. Each image was cropped to only include the filter and converted from color to grayscale. Then, a rectangular region of interest (ROI) was selected in a similar downstream location for each filter, as shown in Figure 11 (top). The ROI location was chosen near the image center where the image is least distorted. The helical cross-step filter was also rotated to maintain a consistent ROI orientation for all of the filters. For these 8 bit images, the grayscale intensity value could range from 0-255. The darkest pixel within the ROI, with a low intensity value, was considered to be ‘not clogged’. The brightest pixel within the ROI, with a high intensity value, was considered to be

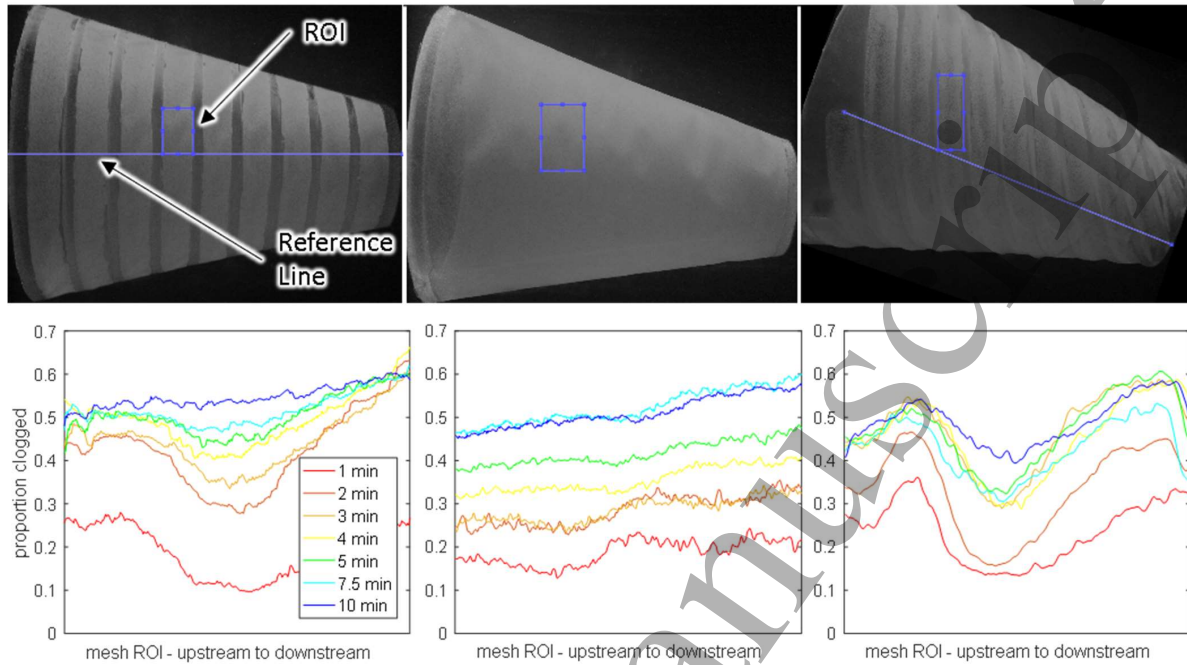


Figure 11: The top row shows the region of interest (ROI) used to quantify the proportion of the filter that was clogged for the: (left) non-helical cross-step filter, (middle) conventional filter, and (right) helical cross-step filter. Reference lines were used for the cross-step filters to accurately locate the ROI. The bottom row shows the corresponding proportion of each filter that was clogged within the ROI, moving from upstream to downstream, for each point in time.

'clogged'. With the intensity range set, the average intensity value was found for each column of pixels within the ROI. The proportion that each filter is clogged is shown in Figure 11 (bottom).

The conventional crossflow filter (Figure 11 middle) became steadily more clogged with time. However, in the two cross-step filters, the shearing effects of the vortices were evident in the center of the slots (Figure 11, left and right). In the cross-step filters, the margins of the slots became clogged, leaving the center of the slots less clogged. After ten minutes, only the vortices in the helical filter were effective at maintaining a less clogged region of mesh near the center of the slot (Figure 11 right).

The vortices in the cross-step filters can be thought of as a passive anti-clogging mechanism because they form even when the filter is statically mounted in the flow tunnel. Although the vortices did keep the center of the slots in the cross-step filters unclogged for a period of time (Figure 10, Figure 11), eventually the center of the slots also began to clog. The slots in this helical filter did extend through the downstream end of the filter, but particles still accumulated in the slots rather than traveling all the way to the downstream end of the filter. Thus, while Figure 11 demonstrates the fluid dynamic effects that the vortices have on clogging, the cross-step models will eventually clog

in the absence of other mechanisms to move particles farther downstream and out of the model. Subsequently, active anti-clogging mechanisms were also considered.

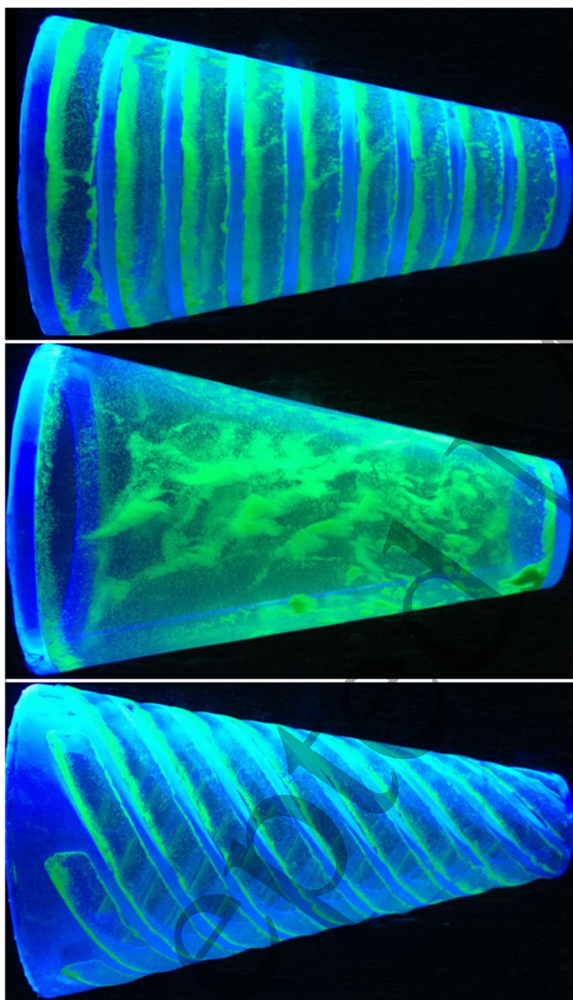
### 3.2.2 Tapping versus Rotation as Active Anti-Clogging Mechanisms:

Two new active anti-clogging mechanisms were employed. The first active mechanism for redistributing deposited particles inside the filter was tapping, or perturbation. After the ten minutes had elapsed in the passive anti-clogging tests (Figure 10), all three filters were tapped several times, with images of the new particle distributions shown in Figure 12. A thin pipe was used to tap the threaded adaptor on the rear of the filter. Particles inside the non-helical cross-step filter were redistributed primarily to the upstream margin of each slot (Figure 12 top). Tapping served as an active movement of the cross-step filter that resuspended trapped particles and enabled the shear layer to scour the mesh systematically. In contrast, redistribution of particles in the conventional net during tapping seemed to be influenced by small wrinkles in the mesh (Figure 12 middle). Lastly, tapping the helical filter caused resuspension of many particles (Supplementary Video 3), which were then transported out the open rear of the helical slots, as shown in Figure 13. Particles that were resuspended but did not travel all the way to the helical slots' exits were redeposited

1  
2  
3 primarily on the upstream margin of each slot, leaving the  
4 middle of the slot clear (Figure 12 bottom).

5 For all filters, tapping had the effect of clearing at least  
6 some of the mesh area, but only the helical filter with the  
7 slots extended to cut through the back wall of the filter has a  
8 mechanism for moving concentrated particles out of the filter  
9 (Figure 13).

10 Rotation of the filter was examined as a second active  
11 mechanism for transporting accumulated particles within the  
12 helical filter. Filter rotation is another example of extending  
13 the bioinspired basis of cross-step filtration beyond the  
14 biologically imposed constraints that limit modes of fish  
15 locomotion, as no ram filter-feeding fish rotate 360° while



49 *Figure 12: Active particle collection by tapping the filters*  
50 *caused particles that had been deposited to be resuspended*  
51 *and eventually redistributed on the mesh for the same three*  
52 *filters used in the passive collection tests: (top) non-helical*  
53 *cross-step filter, (middle) conventional filter without cross-*  
54 *step filtration, and (bottom) helical cross-step filter.*

swimming forward. Tests were performed using a helical  
filter without the slot exits open at the rear. When the slot  
exits are not open at the rear, tapping and rotation can  
redistribute the particles, but they are unable to exit from  
the rear of the filter. The filters were rotated by wrapping a string  
around the threaded adaptor, prior to the test. After particles  
had accumulated on the mesh, the flow tunnel continued to  
operate while the string was pulled from above, rotating the  
filter three to five revolutions on the threaded rod at a rate of  
approximately 0.4 revolutions per second.

When the filter was rotated counter-clockwise (viewed  
from the upstream end) while mounted inside the flow  
tunnel, particles that had accumulated earlier on the mesh  
moved from the upstream end of the filter towards the  
downstream end of the filter, within the helical slots  
(Supplementary Video 4). An image of the redistributed  
particles is shown in Figure 14 for a filter that had previously  
collected particles during a 10-minute passive particle  
collection test. Rotating the filter in the opposite direction,  
clockwise, returned particles to the mesh on the upstream end  
of the filter (Supplementary Video 5).

#### 4. Discussion

This discussion will generally follow the chronological  
testing sequence, starting with iterative tests, followed by the  
clogging tests, advances in our understanding about the  
biological system in light of these experimental results, and  
future development of cross-step filters for the control of  
harmful algal blooms.

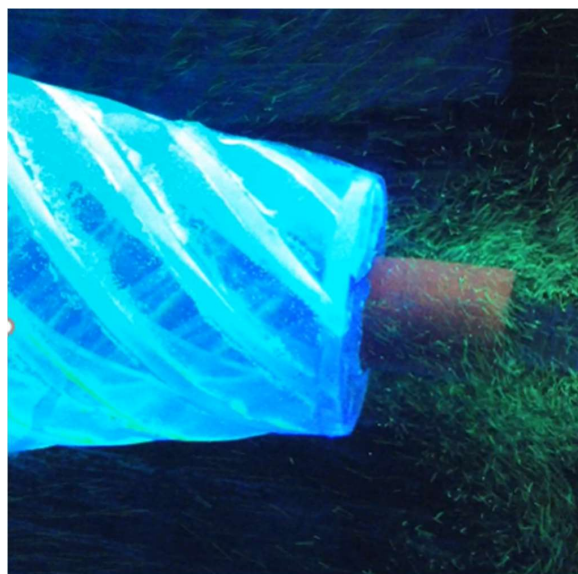


*Figure 13: When the helical slots extended out the back of*  
*the filter, tapping caused particles to be resuspended and*  
*transported out the back of the filter.*

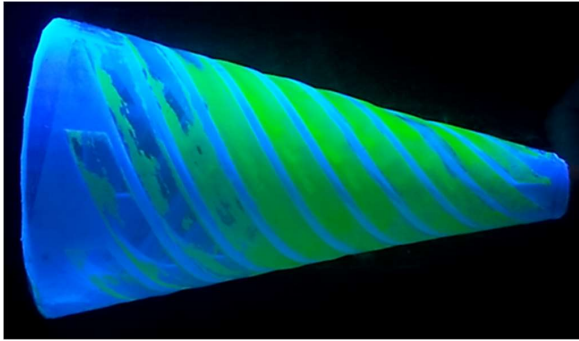


Figure 14: Rotating the helical filter is an active way to transport deposited particles either upstream or downstream, depending on the rotation direction.

**4.1. Iterative Tests:** The iterative tests were used to narrow the many-parameter design space and isolate the influence of individual geometrical parameters. Although the filter geometry appears deceptively simple, a large number of parameters can be varied, including conical angle, slot angle, slot width, rib height, and inlet diameter. The helical versions add yet more parameters including the number of helices, helix pitch, and end-of-slot geometry. Acknowledging the complexity of this design space, it is still much less complex than the actual biological systems from which it is inspired (e.g. Grande and Bemis 1991; Matthews and Parker 1950).

The iterative testing established that a cross-step filter with helical slots can generate a vortex that travels axially within the entire length of the slots. The major lessons learned from the iterative testing were that: (i) the fluid exit ratio is a key design variable that should have a minimum value of approximately 1 for effective vortices to form and cross-step filtration to occur, (ii) cross-step filters can be scaled to have a larger inlet diameter and smaller mesh pore sizes, if the fluid exit ratio remains sufficiently high, (iii) in a helical cross-step filter, the slot angle is affected by conical angle and helix pitch, and can be calculated using Equation 1, (iv) slot angle has a strong effect on axial travel of the vortices within the slots, and (v) the downstream end of the filter and slots must be designed to minimize flow disruption resulting from the dead-end terminus of the filter.

Changing only one of the geometrical parameters often causes changes in the other parameters. For example, decreasing the conical angle increases the fluid exit ratio, which can be desirable. However, a decreased conical angle also causes an increase in the diameter of the dead-end downstream end of the filter, which was associated with vortices that had a smaller diameter and limited axial movement (Figure 7 bottom).

For the helical filters, the slot angle varies along the cone (Equation 1) and is plotted for each helical filter tested in Figure 15. The only filter to successfully generate vortices that traveled continuously from the upstream end to the

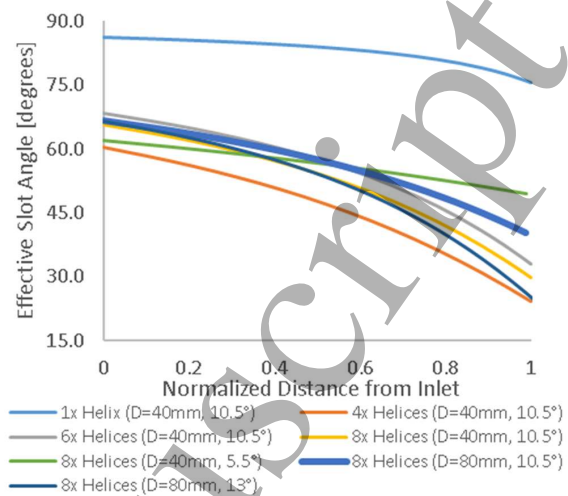


Figure 15: Slot angle from the upstream end to the downstream end of the filter for all of the helical filters tested. The x-axis is the normalized distance from the inlet so that filters of different lengths can be directly compared. The bold line is the only filter that was able to generate a continuous vortex over the entire length of the filter.

downstream end of the filter (Figure 9 bottom) had a slot angle that varied from 66.6° at the inlet to 40.3° at the downstream end. Recall that the design of this filter also removed a source of downstream restriction by extending the helical slots out the filter rear. Perhaps some of the other helical filters would also generate continuous vortex travel along the length of the slots if their slots were similarly extended.

Our results emphasize the importance of considering the fluid exit ratio in the design of cross-step filters. An increase in the entrance area of the model, a decrease in the exit area, and/or a decrease in the open pore area of the mesh will reduce the fluid exit ratio and may adversely affect filtration performance. In our comparison of the models with 100µm mesh versus 140µm mesh (section 3.1.2), effective performance of the filter with the 100µm mesh required adjustments in filter design to increase the fluid exit ratio by increasing the sizes of the slots where fluid exits from the model. However, the sizes of the gaps between filtering structures in filter-feeding fish can be as small as 15-45µm (e.g. Friedland 1985; Cohen and Hernandez 2018), indicating that future experimentation should explore the feasibility of smaller mesh sizes for cross-step filters. Similarly, our flow tunnel speed of 14 cm/s was selected to be comparable with the swimming speed during filtering by paddlefish with mouth sizes roughly comparable to our models. However, larger fish such as basking sharks and whale sharks filter feed while swimming at speeds up to 85-110 cm/s (Motta et al. 2010; Sims 2000), suggesting that further experiments

1  
2  
3 should investigate the effectiveness of cross-step filtration  
4 over a range of flow speeds.

5  
6 **4.2 Clogging Tests:** The clogging tests were used to  
7 compare the clogging behavior of the new helical cross-step  
8 design to both a conventional crossflow filter, and to the  
9 original non-helical cross-step filter. During ten-minute  
10 experiments in a flow tunnel with a high concentration of  
11 particles, all filters became increasingly clogged. The  
12 vortices were able to keep the mesh in the center of the slots  
13 clear for both of the bioinspired filters (Figure 10, top and  
14 bottom), but eventually this part of the mesh began to fill in  
15 as well. Quantitative image analysis established that the  
16 helical cross-step filter was the most successful at  
17 maintaining a less clogged area in the center of the slots  
18 (Figure 11).

19 Tapping all three filters cleared some of the mesh,  
20 allowing them to continue to collect more particles (Figure  
21 12). However, only the helical version with slots extended  
22 through the rear of the filter allowed these particles to be  
23 transported out of the filter during tapping (Figure 13), with  
24 the potential to operate indefinitely without clogging. The  
25 next step is to develop a method for sequestering these  
26 concentrated particles after they exit from the helical filter,  
27 instead of releasing them back into the free stream.

#### 28 **4.3 Rotation as an Active Anti-Clogging Mechanism:**

29 Given the dramatic impact of rotation on particle  
30 concentration and distribution in our helical models (Figure  
31 14), and the different outcomes that we observed for  
32 clockwise versus counter-clockwise rotation (Supplementary  
33 Videos 4 and 5), this active anti-clogging mechanism merits  
34 substantial further experimentation and analysis. In industrial  
35 engineering and fluid mechanics, rotation of a rib-roughened  
36 solid channel in clockwise versus counter-clockwise  
37 directions has complex effects on the flow field that are not  
38 straightforward to predict or model (Narasimhamurthy and  
39 Andersson 2015; Salvagni et al 2017). These complexities  
40 arise primarily from the distinction between the "pressure"  
41 versus the "suction" sides of the ribs during rotation, which is  
42 directly comparable to the distinction between zone 1 versus  
43 zone 3 in cross-step filters (Brooks et al 2018; Sanderson et  
44 al 2016).

45 In cross-step filters, the upstream face of each rib is the  
46 "pressure" side where most fluid exits from the filter, while  
47 the downstream face is the "suction" side where the region of  
48 fluid recirculation is located. In our helical cross-step filters,  
49 the ribs are oriented in a clockwise spiral as viewed from the  
50 entrance of the model. While the flow tunnel pushes fluid  
51 through the filter, we hypothesize that rotation of these  
52 helical filters in a counter-clockwise direction (viewed from  
53 the entrance of the model) enhances the strength of the flow  
54 on the upstream side of each rib because the upstream side is  
55 being rotated into the mainstream flow (i.e., rotated towards

56 the entrance of the model, Supplementary Video 4). This  
57 enhancement on the pressure side of each rib during counter-  
58 clockwise rotation may force the vortex on the downstream  
59 suction side to transport particles towards the back of the  
60 model. In contrast, rotation of the filter in a clockwise  
61 direction could cause a reduction in the strength of the flow  
62 on the upstream side of each rib because the upstream side is  
63 being rotated away from the oncoming mainstream flow (i.e.,  
64 rotated towards the back of the model, Supplementary Video  
65 5). This reduction in the flow that exits from the pressure  
66 side of each rib during clockwise rotation may result in  
67 higher pressures at the back of the model, leading the  
68 vortices to transport particles towards the entrance of the  
69 model. Further experiments are planned to analyze the  
70 transport and concentration of particles during rotation of the  
71 helical model.

#### 72 **4.4 Insights into the Biological System:**

73 Although the design of our helical filter was bioinspired, we found that  
74 careful consideration of the constraints on the biological  
75 system was as instructive as the identification of the novel  
76 biological aspects. Evolution of the basic vertebrate body  
77 plan has led to bilateral symmetry in the external anatomy  
78 and oral cavities of most fish. Recognition of the restrictions  
79 that have been imposed by this biological constraint enabled  
80 us to expand the bioinspired design space and explore the use  
81 of cross-step designs that are asymmetrical or radially  
82 symmetrical. Similarly, as discussed below, identifying the  
83 biological constraints on movement and locomotion in fish  
84 led us to incorporate filter movement in the form of rotation  
85 that does not occur in fish.

86 In our collaborative research, the biology informs the  
87 engineering, and the engineering in turn informs the biology.  
88 Our experimental results, taken both individually and as a  
89 whole, expand our insight into the biological system. Here,  
90 we discuss key outcomes of this synergism between the  
91 engineering and the biological aspects of our study.

##### 92 **4.4.1 Fluid Exit Ratio:**

93 Brooks et al (2018) quantified a new  
94 composite variable that applies to both crossflow and cross-  
95 step filtration in ram filter-feeding fish, termed the fluid exit  
96 ratio. This ratio is calculated as the total open pore area  
97 through which water can exit from the filter, divided by the  
98 area of the inlet through which water enters the filter.  
99 Compared to earlier models for ram filter-feeding fish that  
100 relied on the selection of values for important structural  
101 variables in isolation (e.g. Cheer et al 2012; Paig-Tran et al  
102 2011), the fluid exit ratio is a heuristic variable that  
103 incorporates inlet area, exit area, and percent open pore area  
104 of the filtration surface. The results of our iterative testing  
105 (sections 3.1.1 and 3.1.2 above), combined with the research  
106 of Marshall et al (2018), support the predictions of Brooks et  
107 al (2018) that vortex parameters (e.g., diameter and axial  
108 speed) and cross-step filtration performance will be reduced

1  
2  
3 at fluid exit ratios that are less than approximately 1 in ram  
4 filter-feeding fish.

5 In addition, our research supports the prediction of Brooks  
6 et al (2018) that fluid exit ratios  $\gg 1$  will be associated with  
7 reduced performance in cross-step filters. Our conventional  
8 filter (Figure 10 middle) has a fluid exit ratio of 2.0.  
9 Essentially, this conventional crossflow filter functioned as a  
10 poor cross-step filter because there is only one slot, with a  
11 slot width that is almost the entire length of the filter (k-type  
12 roughness rather than d-type roughness, Liu and Chung  
13 2012). The only mesh in the conventional filter that remained  
14 relatively free of particles in our passive clogging test was  
15 located immediately downstream of the inlet (Figure 10  
16 middle) because the circumference of the inlet served as the  
17 only backward-facing step that generated a vortex as found  
18 in cross-step filtration.

19 **4.4.2 Structural Parameters for Cross-Step Filters:** Our  
20 research suggests that cross-step filtration can continue to be  
21 a viable filtration mechanism as the sizes of the filter  
22 elements are increased proportionately (section 3.1.3). This  
23 result is consistent with estimates reported by Sanderson et al  
24 (2016) that cross-step filtration should be scalable well  
25 beyond the size range of approximately 1 cm to 1 meter  
26 found for the filter inlet diameters of juvenile to adult filter-  
27 feeding fish.

28 The Reynolds number (Re) is a dimensionless ratio of  
29 inertial forces to viscous forces. Thus far, the Re published  
30 for cross-step filters has ranged from approximately 400-600  
31 for the backward-facing steps (Brooks et al 2018; Sanderson  
32 et al 2016). However, backward-facing steps have been  
33 reported to generate a recirculation region in a nonporous  
34 tube or channel across a wide range of Re from  $10^{-4}$  to  $10^5$ ,  
35 calculated using the height of the rib as the characteristic  
36 length dimension (Biswas et al 2004; Chiu and Chien 2011;  
37 Nadge et al 2014). These previous studies on backward-  
38 facing steps indicate that there is the potential for cross-step  
39 filtration to operate over a large range of Re. Our study  
40 supports this hypothesis by expanding the Re range for cross-  
41 step filtration to 1100, calculated using the height of the rib  
42 as the characteristic length dimension.

43 Vortices formed in the non-helical and helical cross-step  
44 filters across a wide range of conical angles ( $\gamma$ ) and slot  
45 angles ( $\alpha$ ) (Table 1, Figure 15). Given the extensive  
46 flexibility of fish to abduct and adduct their branchial arches,  
47 the effects of conical angle and slot angle on vortex  
48 parameters and particle movement deserve further study.  
49 Interestingly, the helical design that generated a continuous  
50 vortex over the entire length of the filter (Figure 9 bottom)  
51 had slot angles ranging from  $66.6^\circ$  at the inlet to  $40.3^\circ$  at  
52 the downstream end (Figure 15), whereas the non-helical  
53 structure of actual paddlefish preserved in filter-feeding  
54 position had slot angles ranging from  $46.4$  to  $15.0$  (Brooks et

al 2018). These results suggest that even smaller slot angles  
might be feasible for cross-step filtration in the helical filters,  
particularly if the rear of the filter is designed with open slots  
as in Figure 9 (bottom).

55 **4.4.3 Transmembrane Pressure Differential:** In contrast  
56 to industrial crossflow filtration (Baker 2012), our models  
57 mimic filter-feeding fish by operating without high pressure  
58 gradients. The transmembrane pressure differential between  
59 the inside and the outside of cross-step models is extremely  
60 small, approximately 11.5 Pa above ambient (Haines and  
Sanderson 2017; Sanderson et al 2016). Effective operation  
at such small transmembrane pressures is essential for ram  
filter-feeding fish in which the power for filtration is  
provided primarily by contraction of body musculature that  
propels the fish as it swims forward with an open mouth.  
This also provides an advantage for cross-step filters that  
could be powered by swimming robotic platforms (Schroeder  
et al 2018).

However, this small transmembrane pressure differential  
also means that the downstream end of cross-step filters and  
slots must be designed to minimize resistance and flow  
disruption resulting from the dead-end terminus of the filter.  
(section 3.1.5). The filter in Figure 9 (top) was scaled to have  
a larger inlet diameter, allowing a larger volume flow rate to  
enter the model. Combined with the relatively small conical  
angle, this scaling of the model in Figure 9 (top) was  
associated with extensive flow disruptions at the downstream  
end of the model, as water was unable to exit adequately  
there. This led to vortices that traveled along the slots in a  
direction that was opposite to the mainstream flow (i.e. from  
the downstream end of the filter to the upstream end, Figure  
9 top). The problem was solved by either increasing the  
conical angle (Figure 9 middle) or designing open slots at the  
downstream end of the filter (Figure 9 bottom). Open slots at  
the terminus of the cross-step filter, through which vortices  
can transport concentrated particles out of the filter, have the  
potential to enable high volume flow rates with reduced  
clogging and low transmembrane pressure differentials.

These results call attention to the structure of the  
downstream end of the oral cavity in ram filter-feeding  
fishes, which has not been described in previous  
morphological studies. Given that our results illustrate the  
potential importance of this morphology, the shape and size  
of the posterior oral cavity in ram filter-feeding fish deserve  
careful analysis. To our knowledge, the oropharyngeal  
cavities of all ram filter-feeding fish are conical rather than  
cylindrical. This is consistent with our finding that the  
conical angle of the models had marked effects on vortex  
parameters and filter clogging (e.g., Figure 7 bottom, Figure  
9). Fish can change the conical angle of the oropharyngeal  
cavity during feeding, which could provide additional control  
over the suspension and transport of particles in vortices.



1  
2  
3 **4.4.4 Anti-Clogging Mechanisms in Fish:** A benefit of  
4 cross-step filtration is that fluid recirculation regions  
5 generated by backward-facing steps serve as a passive anti-  
6 clogging mechanism. However, the mesh in our cross-step  
7 models still clogged eventually during the passive collection  
8 tests (section 3.2.1, Figure 11). Two potential active anti-  
9 clogging mechanisms have been identified in filter-feeding  
10 fish: (1) Filter-feeding fish close their mouth at intervals of  
11 approximately 2-30 s and dynamically reshape movable bony  
12 structures or flexible soft tissue, apparently generating water  
13 flow patterns that could transport collected particles  
14 downstream for swallowing (e.g. Callan and Sanderson  
15 2003; Sanderson et al 1994; Sanderson and Wassersug 1993;  
16 Sims et al 2008). (2) Yaw of the head that occurs during  
17 swimming (Akanyeti et al 2016; Carey and Goldbogen 2017)  
18 can generate fluctuations of flow speed and pressure within a  
19 model fish oral cavity that can transport and concentrate  
20 particles downstream (Haines and Sanderson 2017).

21 We investigated tapping of the filter as an active anti-  
22 clogging mechanism that is a simpler engineering solution  
23 than is found in fish. In addition, we recognized that  
24 movement and locomotor modes in fish may have been  
25 constrained by the evolution of bilateral symmetry in  
26 vertebrates. Therefore, we took advantage of the radial  
27 symmetry in the helical filters and conducted a preliminary  
28 test of the effects of rotation around the anterior-posterior  
29 body axis (section 3.2.2). While fish do not rotate their oral  
30 cavities along the anterior-posterior body axis, filter-feeding  
31 fish do use oscillatory flow and flow reversals (Callan and  
32 Sanderson 2003; Smith and Sanderson 2008), which could  
33 have the effect of altering the flow field at the "pressure"  
34 versus "suction" sides of the ribs (Narasimhamurthy and  
35 Andersson 2015; Salvagni et al 2017).

36 **4.5 Cross-step filter development for the control of**  
37 **harmful algal blooms:** There are intriguing areas for future  
38 work and development of this filtering technology. The  
39 highest priority is the development of a means of capturing  
40 the particles that exit out the downstream end of the helical  
41 filter, which would enable indefinite operation without  
42 clogging. Second, it would also be interesting to employ  
43 'external barriers', which would cover a small area of the  
44 mesh directly next to the upstream margins of the slots. In  
45 previous work (Sanderson et al 2016), these barriers were  
46 effective at not allowing particles to accumulate on the  
47 upstream margins of the slots. Instead, particles were forced  
48 to stay suspended in the vortex, and the axial component of  
49 the vortex transported the particles along the slots.

50 Another aspect of the filter geometry that has not been  
51 thoroughly explored is the angle,  $\beta$ , shown in Figure 1c.  
52 Versions of both the helical and non-helical filters can be  
53 designed with varying beta angles, which is expected to have

an effect on the parameters of the vortex generated in the  
slot.

Our filters were targeted at collecting colonies of harmful  
algae, although the experiments described thus far used  
similarly sized microspheres in place of real algae. Working  
with real algae presents several challenges, including its  
toxicity, its limited availability during the year (peaks in  
August and September), potential for contamination (other  
types of algae or larger organisms, such as zooplankton), and  
underwater visibility.

Real algae have been collected in the field using these  
filters, with an example shown in Figure 16, but it has been  
difficult to observe if the algae are accumulating on the mesh  
in the same way as the particles have in the flow tunnel.  
During our preliminary tests in this turbid low-light  
environment, an underwater camera had to be placed closer  
than 50mm from the mesh for the mesh to be visible. At this  
distance, the camera is likely influencing the flow through  
and around the filter. Furthermore, whenever a submerged  
filter is raised out of the water, this process appears to flush  
some of the algae that has accumulated on the top and sides  
of the filter to the bottom of the filter.

Work will continue refining the tools and techniques to  
study how these filters perform for collecting real algae.



Figure 16: Real algae has been collected in the field and  
initial deposition patterns suggest that cross-step filtration is  
working as expected. Field observations of real algae  
accumulation on the mesh will be challenging to obtain.

## 5. Conclusion and Future Work

The helical design of our bioinspired cross-step filter is an  
improvement over a conventional crossflow filter and a non-  
helical cross-step filter. This new filtration technology  
originated from research on filter-feeding fish and is  
attractive because clogging of the filter can be delayed or  
prevented. Previous filters had been developed that emulated  
the basic cross-step morphology in fish, e.g. had non-helical  
ribs and slots similar to the branchial arches of a paddlefish  
or basking shark (Haines and Sanderson 2017; Brooks et al.  
2018; Marshall et al 2018; Sanderson et al 2016). Our new

filter uses helical slots which enable concentrated particles to be transported via the axial travel of vortices from anywhere along the filter mesh to the downstream end of the filter. This is critical for achieving continuous filtration without clogging.

Our helical filter uses the bioinspired principles of cross-step filtration but extends the idea well beyond the original inspiration because the helical filter is free from biologically imposed constraints such as bilateral symmetry. The helical slots and the lack of longitudinal ribs along the top and bottom of our filter create a radial symmetry that is not present in filter-feeding fish. In turn, this radial symmetry offers the opportunity to implement filter rotation as an active anti-clogging mechanism.

The motivation for developing a new filter was to collect algae colonies from a harmful algal bloom. The size of algae colonies and other physical characteristics drove the experimental design and the adaptation of the cross-step filter. Harmful algal blooms are a global problem and using a filter to physically remove harmful algae would be a more immediate solution than stemming the flow of nutrients and altering other environmental conditions that cause the blooms. Similar cross-step filters could also be employed to remove microplastics from industrial and residential effluent as well as from drinking water.

The helical filter was the product of an iterative design methodology that used water-tracing dye and neutrally buoyant microspheres to qualitatively assess fluid flow and particle collection of the filter. Along with the new helical design, additional outcomes of the iterative testing were an understanding of how varying structural features of the filter influenced fluid flow and filter clogging. Following the iterative design stage, additional clogging tests were performed for select filters at high particle concentrations.

A high priority for future research is the development of a collection system that can retain particles that were captured by and then transported out of the helical filter. This collection system could leverage active anti-clogging strategies developed in this work, including perturbing or rotating the filter. Additionally, the filters must continue to be tested with real algae, which may behave differently in the filter than the algae-sized microspheres.

Lastly, additional quantitative clogging tests will be performed in future work to compare the helical cross-step filter to a conventional, non-bioinspired filter. These tests will further quantify the extent to which the helical filter can operate longer without clogging or can collect more particles than a conventional crossflow filter.

### Acknowledgements

We thank and acknowledge contributions from Patrick Shemanski (University of Toledo), who fabricated the flow tunnel fixture and threaded adaptors, and Dr. Sorin Cioc

(University of Toledo), who granted access to the flow tunnel used for the experiments.

### References

- Akanyeti, O., Thornycroft, P.J.M., Lauder, G.V., Yanagitsuru, Y.R., Peterson, A.N., Liao, J.C., 2016. Fish optimize sensing and respiration during undulatory swimming. *Nat. Commun.* 7, 1–8. <https://doi.org/10.1038/ncomms11044>
- Baker, R.W., 2012. *Membrane Technology and Applications*, 3rd ed. Wiley, West Sussex, UK.
- Biswas, G., Breuer, M., Durst, F., 2004. Backward-facing step flows for various expansion ratios at low and moderate Reynolds numbers. *J. Fluids Eng.* 126, 362–374. <https://doi.org/10.1115/1.1760532>
- Brainerd, E., 2001. Caught in the crossflow. *Nature* 412, 387–388. <https://doi.org/10.1038/35086666>
- Bridgeman, T.B., Chaffin, J.D., Filbrun, J.E., 2013. A novel method for tracking western Lake Erie *Microcystis* blooms, 2002–2011. *J. Great Lakes Res.* 39, 83–89. <https://doi.org/10.1016/j.jglr.2012.11.004>
- Brooks, H., Haines, G.E., Lin, M.C., Sanderson, S.L., 2018. Physical modeling of vortical cross-step flow in the American paddlefish, *Polyodon spathula*. *PLoS One* 13, 1–25. <https://doi.org/10.1371/journal.pone.0193874>
- Callan, W.T., Sanderson, S.L., 2003. Feeding mechanisms in carp: crossflow filtration, palatal protrusions and flow reversals. *J. Exp. Biol.* 206, 883–892. <https://doi.org/10.1242/jeb.00195>
- Carey, N., Goldbogen, J.A., 2017. Kinematics of ram filter feeding and beat–glide swimming in the northern anchovy *Engraulis mordax*. *J. Exp. Biol.* 220, 2717–2725. <https://doi.org/10.1242/jeb.158337>
- Chaffin, J.D., Bridgeman, T.B., Heckathorn, S.A., Mishra, S., 2011. Assessment of *Microcystis* growth rate potential and nutrient status across a trophic gradient in western Lake Erie. *J. Great Lakes Res.* 37, 92–100. <https://doi.org/10.1016/j.jglr.2010.11.016>
- Cheer, A., Cheung, S., Hung, T.C., Piedrahita, R.H., Sanderson, S.L., 2012. Computational Fluid Dynamics of Fish Gill Rakers During Crossflow Filtration. *Bull. Math. Biol.* 74, 981–1000. <https://doi.org/10.1007/s11538-011-9709-6>
- Chiu, J.-J., Chien, S., 2011. Effects of disturbed flow on vascular endothelium: pathophysiological basis and clinical perspectives. *Physiol. Rev.* 91, 327–387. <https://doi.org/10.1152/physrev.00047.2009>
- Cohen, K.E., Hernandez, L.P., 2018. Making a master filterer: ontogeny of specialized filtering plates in silver carp (*Hypophthalmichthys molitrix*). *J. Morphol.* 925–935. <https://doi.org/10.1002/jmor.20821>
- Cohen, K.E., Hernandez, L.P., Crawford, C.H., Flammang, B.E., 2018. Channeling vorticity: modeling the filter-feeding mechanism in silver carp using  $\mu$ CT and 3D PIV. *J. Exp. Biol.* 221, 1–12. <https://doi.org/10.1242/jeb.183350>
- Friedland, K., 1985. Functional morphology of the branchial basket structures associated with feeding the Atlantic menhaden, *Brevoortia tyrannus* (Pisces: Clupeidae). *Copeia* 4, 1018–1027.
- Grande, L., Bemis, W.E., 1991. Osteology and phylogenetic relationships of fossil and recent paddlefishes (Polyodontidae) with comments on the interrelationships

- of Acipenseriformes. *Vertebr. Paleontol. Mem.* 1 11, 1–121.
- Haines, G.E., Sanderson, S.L., 2017. Integration of swimming kinematics and ram suspension feeding in a model American paddlefish, *Polyodon spathula*. *J. Exp. Biol.* 220, 4535–4547. <https://doi.org/10.1242/jeb.166835>
- Imbrogno, J., Belfort, G., 2016. Membrane Desalination: Where Are We, and What Can We Learn from Fundamentals? *Annu. Rev. Chem. Biomol. Eng.* 7, 29–64. <https://doi.org/10.1146/annurev-chembioeng-061114-123202>
- International Joint Commission, 2014. A Balanced Diet for Lake Erie: Reducing Phosphorus Loadings and Harmful Algal Blooms. Report of the Lake Erie Ecosystem Priority (LEEP)
- Jaffrin, M.Y., 2012. Hydrodynamic Techniques to Enhance Membrane Filtration. *Annu. Rev. Fluid Mech.* 44, 77–96. <https://doi.org/10.1146/annurev-fluid-120710-101112>
- Kudela R.M., Berdalet, E., Bernard, S., Burford, M., Fernand, L., Lu, S., Roy, S., Tester, P.A., Usup, G., Magnien, R., Anderson, D.M., Cembella, A., Chinain, M., Hallegraef, G., Reguera, B., Zingone, A., Enevoldsen, H., Urban, E., 2015. Harmful Algal Blooms: A Scientific Study for Policy Makers. IOC/UNESCO, Paris (IOC/INF-1320)
- Leonardi, S., Orlandi, P., Smalley, R.J., Djenidi, L., Antonia, R.A., 2003. Direct numerical simulations of turbulent channel flow with transverse square bars on one wall. *J. Fluid Mech.* 491, 229–238. <https://doi.org/10.1017/S0022112003005500>
- Liu, C., Chung, T.N.H., 2012. Forced convective heat transfer over ribs at various separation. *Int. J. Heat Mass Transf.* 55, 5111–5119. <https://doi.org/10.1016/j.ijheatmasstransfer.2012.05.012>
- Marshall, L., Schroeder, A., Trease, B., 2018. Comparing Fish-Inspired Ram Filters for Collection of Harmful Algae, in: Proceedings of the ASME 2018 International Mechanical Engineering Congress and Exposition IMECE2018. pp. 1–9.
- Matthews, L.H., Parker, H.W., 1950. Notes on the Anatomy and Biology of the Basking Shark (*Cetorhinus maximus* (Gunner)). *P. Zool. Soc. L.* 120, 535–576.
- Motta, P.J., Maslanka, M., Hueter, R.E., Davis, R.L., de la Parra, R., Mulvany, S.L., Habegger, M.L., Strother, J.A., Mara, K.R., Gardiner, J.M., Tyminski, J.P., Zeigler, L.D., 2010. Feeding anatomy, filter-feeding rate, and diet of whale sharks *Rhincodon typus* during surface ram filter feeding off the Yucatan Peninsula, Mexico. *Zoology* 113, 199–212. <https://doi.org/10.1016/j.zool.2009.12.001>
- Nadge, P.M., Govardhan, R.N., 2014. High Reynolds number flow over a backward-facing step : structure of the mean separation bubble. *J. Exp. Fluids* 55, 1–22. <https://doi.org/10.1007/s00348-013-1657-5>
- Nakamura, T., Adachi, Y., Suzuki, M., 1993. Flotation and sedimentation of a single *Microcystis* floc collected from surface bloom. *Water Res.* 27, 979–983. [https://doi.org/10.1016/0043-1354\(93\)90061-L](https://doi.org/10.1016/0043-1354(93)90061-L)
- Narasimhamurthy, V.D., Andersson, H.I., 2015. Turbulence statistics in a rotating ribbed channel. *Int. J. Heat Fluid Flow* 51, 29–41. <https://doi.org/10.1016/j.ijheatfluidflow.2014.10.008>
- Paerl, H.W., 2014. Mitigating Harmful Cyanobacterial Blooms in a Human- and Climatically-Impacted World. *Life* 2014, 4, 988–1012. <https://doi.org/10.3390/life4040988>
- Paig-Tran, E.W.M., Bizzarro, J.J., Strother, J.A., Summers, A.P., 2011. Bottles as models: predicting the effects of varying swimming speed and morphology on size selectivity and filtering efficiency in fishes. *J. Exp. Biol.* 214, 1643–1654. <https://doi.org/10.1242/jeb.048702>
- Paig-Tran, E.W.M., Kleinteich, T., Summers, A.P., 2013. The filter pads and filtration mechanisms of the devil rays: Variation at macro and microscopic scales. *J. Morphol.* 274, 1026–1043. <https://doi.org/10.1002/jmor.20160>
- Rowe, M.D., Anderson, E.J., Wynne, T.T., Stumpf, R.P., Fanslow, D.L., Kijanka, K., Vanderploeg, H.A., Strickler, J.R., Davis, T.W., 2016. Vertical distribution of buoyant *Microcystis* blooms in a Lagrangian particle tracking model for short-term forecasts in Lake Erie. *J. Geophys. Res. Ocean.* 121, 5296–5314. <https://doi.org/10.1002/2016JC011720>
- Salvagni, A., Borello, D., Rispoli, F., Hanjalić, K., 2017. Large-eddy simulations of heat transfer in asymmetric rib-roughened ducts: Effects of rotation. *Int. J. Heat Fluid Flow* 68, 373–385. <https://doi.org/10.1016/j.ijheatfluidflow.2017.09.019>
- Sanderson, S., Wassersug, R., 1990. Suspension-feeding vertebrates. *Sci Am.* 262, 96–101.
- Sanderson, S.L., Cech Jr., J.J., Cheer, A.Y., 1994. Paddlefish buccal flow velocity during ram suspension feeding and ram ventilation. *J. Exp. Biol.* 186, 145–156.
- Sanderson, S.L., Cheer, A.Y., Goodrich, J.S., Graziano, J.D., Callan, W.T., 2001. Crossflow filtration in suspension-feeding fishes. *Nature* 412, 439–441. <https://doi.org/10.1038/35086574>
- Sanderson, S.L., Roberts, E., Lineburg, J., Brooks, H., 2016. Fish mouths as engineering structures for vortical cross-step filtration. *Nat. Commun.* 7, 11092. <https://doi.org/10.1038/ncomms11092>
- Sanderson, S.L., Wassersug, R.W., 1993. Convergent and alternative designs for vertebrate suspension feeding. The Skull: Functional and Evolutionary Mechanisms, Vol. 3 (eds. Hanken, J., Hall, B.K.), 37–112. Univ. of Chicago Press, Chicago.
- Schroeder, A., Trease, B., Arsie, A., 2018. Balancing Robot Swarm Cost and Interference Effects by Varying Robot Quantity and Size. *Swarm Intell.* <https://doi.org/DOI:10.1007/s11721-018-0161-1>
- Sims, D.W., 2000. Filter-feeding and cruising swimming speeds of basking sharks compared with optimal models: they filter-feed slower than predicted for their size. *J. Exp. Mar. Biol. Ecol.* 249, 65–76.
- Sims, D.W., Southall, E.J., Humphries, N.E., Hays, G.C., Bradshaw, C.J.A., Pitchford, J.W., James, A., Ahmed, M.Z., Brierley, A.S., Hindell, M.A., Morritt, D., Musyl, M.K., Righton, D., Shepard, E.L.C., Wearmouth, V.J., Wilson, R.P., Witt, M.J., Metcalfe, J.D., 2008. Scaling Laws of Marine Predator Search Behaviour. *Nature* 451, 1098–1102. <https://doi.org/10.1038/nature06518>
- Smith, J.C., Sanderson, S.L., 2008. Intra-oral flow patterns and speeds in a suspension-feeding fish with gill rakers

1  
2 removed versus intact. Biol. Bull. 215, 309–318.

3 <https://doi.org/10.2307/25470714>

4 Stel, H., Franco, A.T., Junqueira, S.L.M., Erthal, R.H., Mendes, R.,  
5 Gonçalves, M.A.L., Morales, R.E.M., 2012. Turbulent  
6 Flow in D-Type Corrugated Pipes: Flow Pattern and  
7 Friction Factor. J. Fluids Eng. 134, 121202.

8 <https://doi.org/10.1115/1.4007899>

9 Zhou, G., Wang, K.P., Liu, H.W., Wang, L., Xiao, X.F., Dou, D.D.,  
10 Fan, Y.B., 2018. Three-dimensional polylactic  
11 acid@graphene oxide/chitosan sponge bionic filter:

12 Highly efficient adsorption of crystal violet dye. Int. J.

13 Biol. Macromol. 113, 792–803.

14 <https://doi.org/10.1016/j.ijbiomac.2018.02.017>

15 Zhu, W., Li, M., Luo, Y., Dai, X., Guo, L., Xiao, M., Huang, J.,  
16 Tan, X., 2014. Vertical distribution of *Microcystis* colony  
17 size in Lake Taihu: Its role in algal blooms. J. Great

18 Lakes Res. 40, 949–955.

19 <https://doi.org/10.1016/j.jglr.2014.09.009>  
20  
21  
22  
23  
24  
25  
26  
27  
28  
29  
30  
31  
32  
33  
34  
35  
36  
37  
38  
39  
40  
41  
42  
43  
44  
45  
46  
47  
48  
49  
50  
51  
52  
53  
54  
55  
56  
57  
58  
59  
60